FDTD Simulations of TEM Horns and the Implications for Staircased Representations

John B. Schneider and Kurt L. Shlager, *Member, IEEE*

***Abstract*— Two-dimensional (2-D) TEM horns are modeled using the finite-difference time-domain (FDTD) method. The boundary walls are perfect electric conductors and one wall, which does not align with the Cartesian grid, is approximated using a staircased representation. By carefully comparing the FDTD results to those of the analytic solution, one can make conclusions about the coarseness with which a boundary can be represented. It is found that staircasing errors are small when the staircase diagonal (the hypotenuse of the right triangle created by the stairstep) is smaller than half a wavelength at the highest significant frequency in the excitation. This rule-of-thumb is put forward as a necessary condition for the discretization of general problems. Results are also provided for some simple FDTD schemes that are designed to reduce staircasing errors. By using large aspect-ratio cells, a grid can be constructed that satisfies the rule-of-thumb given above. While this approach eliminates general staircasing errors, some errors persist owing to the presence of step discontinuities immediately adjacent to the horn feed. These errors can be further reduced by using a cell-splitting approach. It is shown that the contour path FDTD technique can be used to eliminate nearly all staircasing errors, while some additional improvement is shown to be provided by using a stabilized contour path FDTD approach. Finally, a recently proposed conformal technique that permits simple implementation is shown to provide results comparable with those of the stabilized contour path approach.**

***Index Terms*—FDTD methods, horn antennas.**

I. Introduction

INHERENT in the original Cartesian grid finite-difference time-domain (FDTD) method is a stairstep representation of material boundaries [1]. This approximation can lead to inaccurate solutions and has prompted the development of a wide range of schemes designed to reduce or eliminate staircasing errors (e.g., [2]–[6]). Unfortunately, these alternative approaches have costs, both in terms of computational overhead and algorithm complexity, above that of the original FDTD scheme. Previously, there has been some analysis of staircasing errors associated with perfectly conducting boundaries. For example, Cangellaris and Wright [7] rigorously analyzed the staircased representation of a planar surface tilted 45° to the grid, while Holland [8] analyzed errors associated with a slightly tilted planar scatterer. However, the analysis in these papers did not give guidelines for avoiding staircasing errors that would hold for general problems in which a staircase approximation is used.

In this paper, two-dimensional (2-D) narrow-angled horns are used as a test bed to study staircasing errors. A voltage source excites a TE wave and the field calculated at an observation point is compared to the analytic solution. For the analytic solution to hold, the driving feed voltage must be very near the horn apex and this requires (as discussed in Section II) special consideration in the FDTD implementation. Section III gives a comparison of the analytic solution with those obtained using a traditional Cartesian-grid, stairstepped solution. It is found that general staircasing errors are small provided that the horn walls are discretized such that the staircase diagonal is less than half a wavelength of the highest significant frequency in the excitation. The word "general," in connection with the staircasing errors, is used here to distinguish between errors associated with the modeling of the horn walls and those associated with the implementation of the feed. We consider the errors associated with the wall "general" while those associated with the implementation of the feed are specific to this particular horn geometry.

Section IV shows the results obtained using simple modifications to the original FDTD scheme that help alleviate staircasing errors. These schemes include the cell-splitting scheme that has been described by (among others) Mezzanotte *et al.* [9], the contour path technique [4], [10], and the method recently presented by Dey and Mittra [11] and Dey *et al.* [12]. It is found that large aspect-ratio cells can be used to reduce general staircasing errors. However, owing to their inherent coarseness, these cells do not, by themselves, allow for a completely accurate implementation of the horn feed. By splitting these cells accurate results can be obtained. The contour path approach is found to provide high-fidelity results. It is shown that a modified contour-path technique [13], which was put forward to ensure stability of the technique, provides additional accuracy above that of the original scheme. The Dey method, which is arguably the simplest conformal method to implement, is found to provide results comparable to that of the modified contour path scheme.

Although the analysis presented in this paper is done in two dimensions, the results are consistent with those seen in the study of three-dimensional (3-D) horn antennas [14]. The material presented here is, in fact, a continuation of the work

Manuscript received January 31, 1997; revised August 14, 1997. This work was supported in part by the Office of Naval Research Code 321OA.

J. B. Schneider is with the School of Electrical Engineering and Computer Science, Washington State University, Pullman, WA 99164 USA.

K. L. Shlager is with the Lockheed Martin Missiles & Space Co., Sunnyvale, CA 94089 USA.

Publisher Item Identifier S 0018-926X(97)09050-9.

presented in [14, Appendix] that was itself used to determine accurate discretizations for 3-D horns.

II. Analytic Solution and Feed Implementation

Consider a horn, shown in Fig. 1(a), that is driven by a voltage source $v(t)$ located a distance r_0 from the horn apex. The horn plates form an angle α and are assumed to continue indefinitely. Assuming transverse electromagnetic (TEM) propagation, a general solution for E_ϕ at a distance r from the apex at an angular frequency ω, which satisfies Maxwell's equations and the radiation and boundary conditions, is given by

$$E_\phi(r,\omega) = -j\eta A(\omega) H_1^{(2)}(kr) \tag{1}$$

where η is the characteristic impedance of free space, k is the wave number, $H_1^{(2)}$ is the first-order Hankel function of the second kind, and the coefficient A is yet to be determined. Restricting, for the time being, kr to be much less than unity and employing the small argument approximation of the Hankel function, the field is given by

$$E_\phi(r,\omega) = \frac{2\eta}{\pi kr} A(\omega). \tag{2}$$

Since the field is independent of ϕ, the voltage at a distance r from the apex can be expressed as $V(r,\omega) = -\alpha r E_\phi(r,\omega)$. Using this relation in (2) yields the following relation between the coefficient A and the voltage:

$$A(\omega) = -\frac{\pi k}{2\eta\alpha} V(r,\omega). \tag{3}$$

Note that although A is independent of r, this simple relationship between A and V does not imply that the voltage is similarly independent of position since it only holds when the small argument approximation of the Hankel function holds. Since the voltage source is close to the apex (i.e., $kr_0 \ll 1$), r can be set to r_0 in (3) and used in (1) to obtain

$$E_\phi(r,\omega) = -\frac{\pi}{2\alpha c}(j\omega)^2 V(r_0,\omega)\frac{1}{-j\omega} H_1^{(2)}(\omega r/c) \tag{4}$$

where k has been changed to ω/c, c is the speed of light, and the expression has been multiplied and divided by $-j\omega$. The time-domain representation of this solution is the convolution of the second derivative of the voltage at the feed and the kernel function given by the time-domain representation of $1/(-j\omega)H_1^{(2)}(\omega r/c)$. Specifically, the time-domain solution can be written as

$$E_\phi(r,t) = -\frac{1}{\alpha r}\int_{-\infty}^{t} v''\Big(u - \frac{r}{c}\Big) \cdot \left[\Big(t + \frac{r}{c} - u\Big)^2 - \Big(\frac{r}{c}\Big)^2\right]^{1/2} du \tag{5}$$

where v'' is the second derivative of the voltage at the feed. This convolution integral can be integrated numerically to obtain the field at any point within the horn.

Consider, as shown in Fig. 1(b), a uniform Cartesian grid FDTD representation of a horn with a 12:1 slope ($\alpha \approx 4.76$ degrees). Assuming $\Delta x = \Delta y = \delta$, the simplest

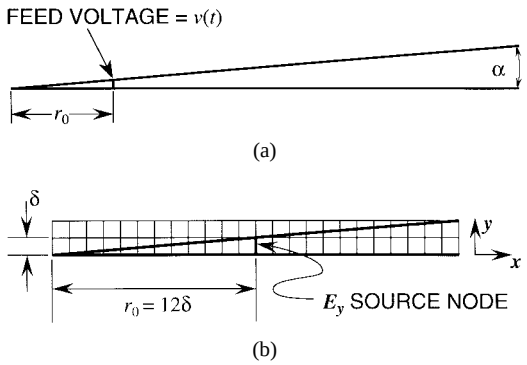

Fig. 1. (a) Geometry of the physical horn. (b) FDTD representation (staircasing not shown).

implementation of the feed appears to be to set the first vertical electric field node that is completely between the horn plates to the voltage divided by the negative of the node length, i.e., $E_y^n = -v(n\Delta t)/\delta$, where n is the time step. However, such an implementation will not generally satisfy the requirement that $kr_0 \ll 1$ for all the spectral components of interest. Using the horn of Fig. 1(b) as an example, kr_0 is $24\pi/(\lambda/\delta) \approx 75.4/$ (cells per wavelength). In order for this to be much less than unity, the cells per wavelength would have to be prohibitively large. (Note that for narrow-angle horns, the difference between E_y and E_ϕ is small for the E_y nodes along the bottom plate. Hence, for these nodes, E_y and E_ϕ will be used interchangeably.)

Fortunately, there are several ways to implement the feed so that the FDTD results can be compared directly to the analytic solution. In [14], a nonuniform, "ballooning" mesh was used. In this approach, small cells are used in the vicinity of the horn apex. The size of the cells close to the apex are chosen to ensure that kr_0 is much less than unity for the first E_y that falls completely between the horn plates. Moving away from the apex, the cell sizes are gradually increased until they have the desired size. The drawbacks of this approach are that the temporal step size is dictated by the smallest cell in the grid (and, hence, may be much less than would be used in a uniform grid solution) and the grid is distorted "globally" to accommodate the small cells near the apex. For instance, this distortion requires that the first few rows of nodes above the bottom plate have small heights regardless of their distance from the apex (only the widths of the nodes in these rows increase away from the apex).

A second approach that can be used to implement the feed uses the uniform grid shown in Fig. 1(b); however, the source is not driven directly by a scaled version of the voltage. Instead, the source node is set equal to the field obtained from the analytic expression. In other words, the node identified as the source node in Fig. 1(b) is set equal to the convolution integral given by (5) where r is the distance from the center of the source node to the apex (which would be $\sqrt{12^2 + (1/2)^2}\delta$ for a 12:1 horn). By analytically propagating the field from a voltage source that is implicitly close to the apex to the source node, the restriction on the location of the voltage source is automatically satisfied. This approach permits the study of uniform grids with little concern for the size of the initial

source node. However, this approach does have the drawback of requiring the calculation of a convolution integral at each time step.

A third approach that provides essentially the same accuracy as the previous approach, but is simpler to implement, is to use an auxiliary one-dimensional (1-D) cylindrical FDTD solution to model propagation in the horn. The cylindrical grid solution is inherently free of any staircasing errors and can be driven by a voltage source located at the first E_ϕ node (which can be very close to the apex). To guarantee that there are essentially no numerical errors in the cylindrical grid solution, the spatial step size can be chosen to be a fraction of that in the 2-D Cartesian grid. Setting the cylindrical grid spatial step size so that a integer multiple of them equals one Cartesian step permits simple alignment (spatial correspondence) of the two grids.

For the work presented here, an auxiliary 1-D cylindrical grid was used to determine the field present at the source node. (Also, the spectral-domain results presented in the next sections were obtained using a cylindrical grid where the fields were recorded at the appropriate observation point. Those results were verified by comparing to those obtained using the convolution integral.) Specifically, the following update equations were used for the auxiliary grid

$$E_\phi^n(1) = -\frac{1}{\alpha\Delta\rho}v(n\Delta t) \tag{6}$$

$$E_\phi^{n+1}(i) = E_\phi^n(i) - \frac{\Delta t}{\epsilon\Delta\rho} \cdot \left[H_z^{n+1/2}(i) - H_z^{n+1/2}(i-1)\right] \tag{7}$$

$$H_z^{n+1/2}(i) = H_z^{n-1/2}(i) - \frac{\Delta t}{\mu(2i+1)\Delta\rho} \cdot [(2i+2)E_\phi^n(i+1) - 2iE_\phi^n(i)] \tag{8}$$

where $E_\phi^n(i) = E_\phi(i\Delta\rho, n\Delta t)$ and $H_z^{n+1/2}(i) = H_z((i+1/2)\Delta\rho, (n+1/2)\Delta t)$. It was found, for the cases studied here, that using spatial and temporal step sizes in the cylindrical grid that were one fourth of that in the corresponding 2-D grid gave results indistinguishable from those obtained using the convolution integral. Thus, $\Delta\rho$ was set equal to $\delta/4$ and Δt was set to $\delta/(4c\sqrt{2})$. The temporal step in the cylindrical grid was set to one fourth the Courant number in two dimensions in order to provide simple temporal synchronization of the grids. To illustrate the implementation of the Cartesian grid source node, consider a horn with a $12:1$ slope. In the Cartesian grid, the source node is located 12δ from the apex. Identifying this node as $E_y^n(12,1)$ (where the argument indicates the node is located 12 horizontal steps from the apex and along the first row of nodes), the source is realized by setting $E_y^n(12,1)$ equal to $E_\phi^{4n}(48)$, as found in the cylindrical grid.

The subsequent analysis can be performed using any number of voltage functions. We merely require that the signal be fairly broad-band. The differentiated Gaussian pulse is used here. Specifically, the time-domain representation is given by

$$v(t) = -\frac{t}{\tau_p}\exp\left(-\frac{1}{2}\left(\frac{t^2}{\tau_p^2} - 1\right)\right) \tag{9}$$

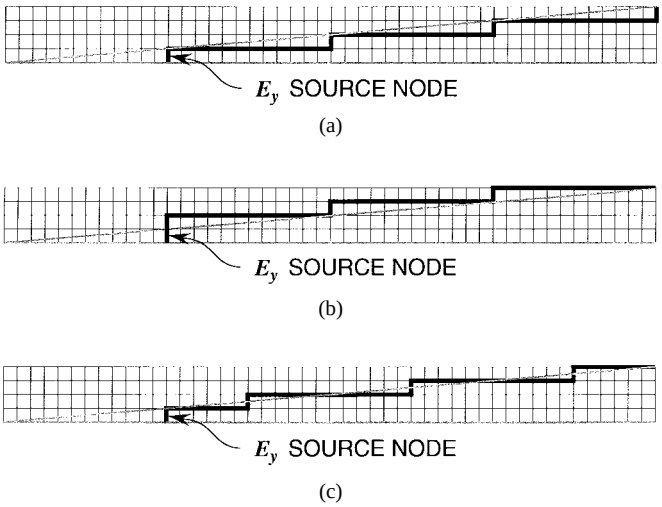

Fig. 2. Staircased representations of the horn. (a) Outside staircase. (b) Inside staircase. (c) Average staircase.

where τ_p is a time constant. Taking the Fourier transform yields

$$V(\omega) = -j\tau_p^2\omega\sqrt{2\pi}\exp\left(-\frac{1}{2}(\tau_p^2\omega^2 - 1)\right). \tag{10}$$

For the sake of concreteness, we choose a time constant of $\tau_p = 65$ ps (but, ultimately, the conclusions will be independent of the time constant chosen). This value of τ_p yields a spectrum which has peak energy at 2.45 GHz and nearly all the energy falls below 9.0 GHz.

III. Uniform Cartesian Grid

This section presents the results obtained using a uniform Cartesian grid to model narrow-angle horns. For the sake of brevity, the discussion will focus on a horn with a $12:1$ slope. The spatial step size is 2 mm, yielding approximately 17 cells per wavelength at the "highest" frequency of the pulse (9 GHz) and approximately 61 cells per wavelength at the peak frequency (2.45 GHz). The time step is at the Courant limit. The observation point at which the FDTD and analytic results will be compared is 5 cm from the apex. For this level of discretization and for this observation point, numerical dispersion and anisotropy are negligible.

Although restricting ourselves here to a uniform grid, the sloped wall of the horn can be approximated in a number of ways. First, we define a cell as an H_z node together with the four surrounding electric field nodes. Thus, referring to the grids shown in Fig. 2, a cell corresponds to a square where H_z nodes are located in the center of each square. We define an outside staircase by treating a cell as completely within metal if any portion of the cell is in metal. (An outside staircase is one in which the staircased approximation of the conductor wall lies completely outside of the metal as defined by the true physical boundary.) Fig. 2(a) shows the outside staircase representation of a $12:1$ horn. Alternatively, as shown in Fig. 2(b), we define an inside staircase as one where a cell is treated as being between the horn plates (i.e., in free-space) if any portion of the cell is between the plates. (An inside

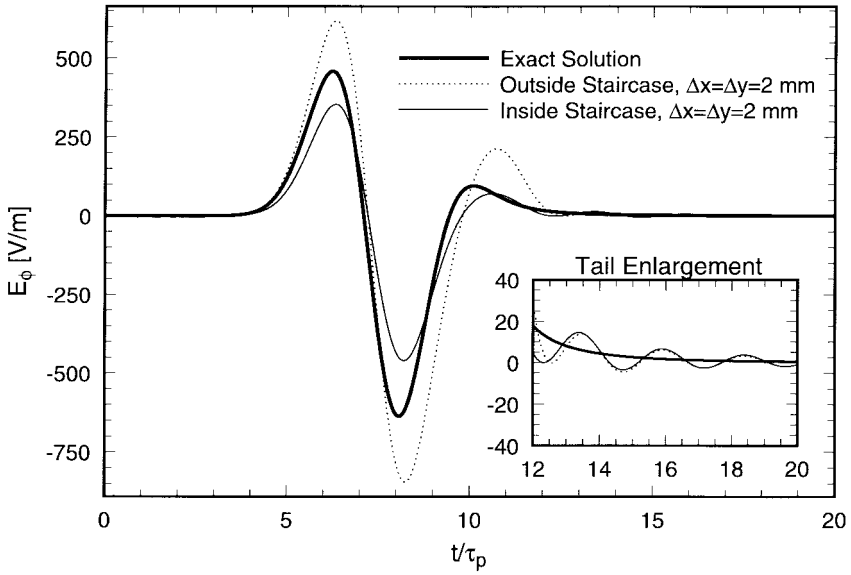

Fig. 3. Electric field 5 cm from the apex using an outside and inside staircase. $\Delta x = \Delta y = 2$ mm.

staircase is one in which the staircased approximation of the conductor wall falls completely within the metal as defined by the true physical boundary.) In both realizations the source node is the same. Although the source node is not collocated with the voltage feed, it will subsequently be identified as the feed node.

Fig. 3 shows, on a normalized time scale, the electric field found 5 cm from the apex using an outside and inside staircase. The inset box shows an enlargement of the late-time signal. The outside staircase clearly over predicts the field while the inside staircase under predicts. As significant as these errors are, they do not (in themselves) provide much information about general staircasing errors. Instead, these errors further point to the sensitivity of this test bed to the implementation of the feed. When using an outside staircase, the feed node first couples into a parallel plate waveguide of 12 cells before encountering any hint of the true geometry. This waveguide has the effect of displacing the feed closer to the observation point and, hence, the fields are over predicted. Using the inside staircase, the feed node is adjacent to a step discontinuity that thus behaves as a horn that is wider than the true horn; hence, the fields are under predicted. What is significant here is the ringing in the tail of the pulse—these errors are directly attributable to general staircasing errors and will be analyzed further in a moment. Unfortunately, the large errors throughout the main portion of the pulse can mask these errors.

The results obtained for an outside and inside staircase naturally lead to the definition of an "average" staircase where a cell is either in metal or free-space depending upon the location of the center of the cell (i.e., the material in which the H_z node is located). An average staircase representation of a 12 : 1 horn would, as shown in Fig. 2(c), have six cells between the feed node and the first stairstep and would, thereafter, have 12 cells between stairsteps. The field found at 5 cm for an average staircase is shown in Fig. 4. Over the main portion of this pulse, this staircase provides much better results than either the outside or inside staircase, but now the ringing in the tail is more pronounced. A simple enhancement, which can be found described in [15, Sect. 10.3.1], is obtained by "splitting" the cells associated with the step discontinuities. These cells are split along their diagonals so that the metal is assumed to pass directly through the H_z nodes at the center of the cell. For each such split cell, three nonzero field components are created and the corresponding H_z has its update equation modified by a factor two compared to that of an unsplit cell. The results obtained using an average staircase with cell splitting at the step discontinuities are also shown in Fig. 4. Cell splitting reduces the amount of overshoot in the main pulse and reduces, but does not eliminate, the amount of ringing in the tail. (Note that the cell splitting used here does not involve any global distortion of the grid nor does it involve splitting all cells adjacent to the metal. This is in contrast to the scheme described by Mezzanotte *et al.* [9], which will be discussed in the next section.)

Since the best results appear to be those obtained using an average staircase with cell splitting, we focus our attention on those. By taking the Fourier transform of the FDTD signal, one finds significant error near 6.25 GHz. This error, which appears as a spike in the spectrum, is associated with the ringing that is present in each of the results obtained thus far. However, such spectral plots are not useful in themselves. Instead, to facilitate the analysis, it is convenient first to define Δs as the stairstep diagonal length, which, as shown in Fig. 5, corresponds to the hypotenuse of the stairstep. Plotting the normalized spectrum of the results against the frequency scaled by $\Delta s/c$ yields, as shown in Fig. 6, the spectrum versus $\Delta s/\lambda$. The spike is located almost exactly at $\Delta s = \lambda/2$. Some of the ripples in the spectrum above $\Delta s = \lambda/2$ are attributed to the aliasing caused by halting the simulation prior to the signal ringing down to zero. Simulations were terminated after 8192 time steps (corresponding roughly to $t = 600\tau_p$) and the computational domain was made large enough to isolate causally the end of the computational domain from the observation point. Thus,

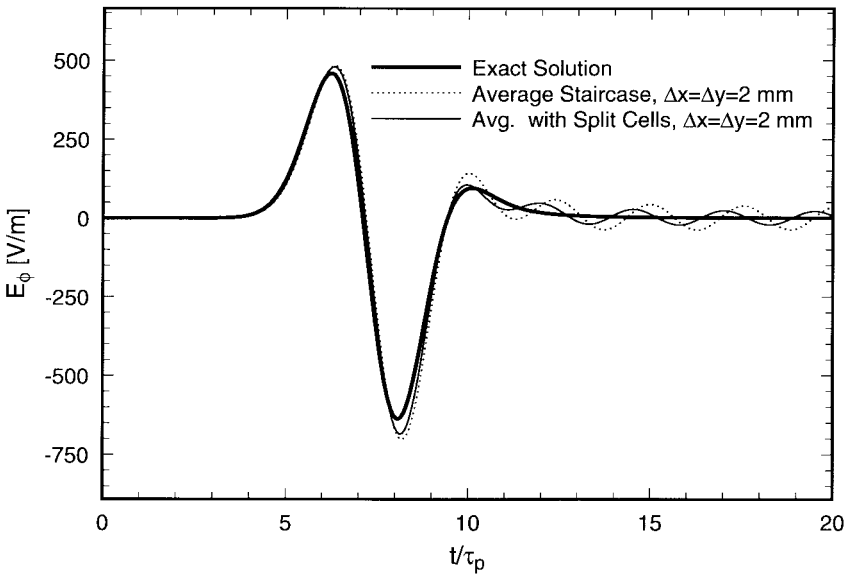

Fig. 4. Electric field 5 cm from the apex using an average staircase and an average staircase with cell splitting (every twelfth cell split). $\Delta x = \Delta y = 2$ mm.

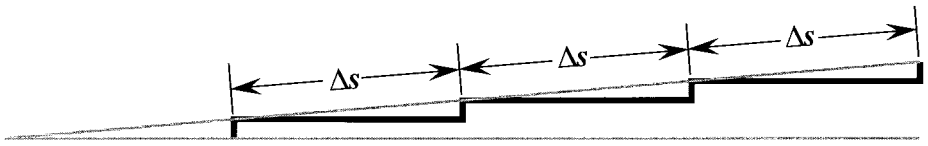

Fig. 5. Δs is defined to be the length of the stairstep diagonal.

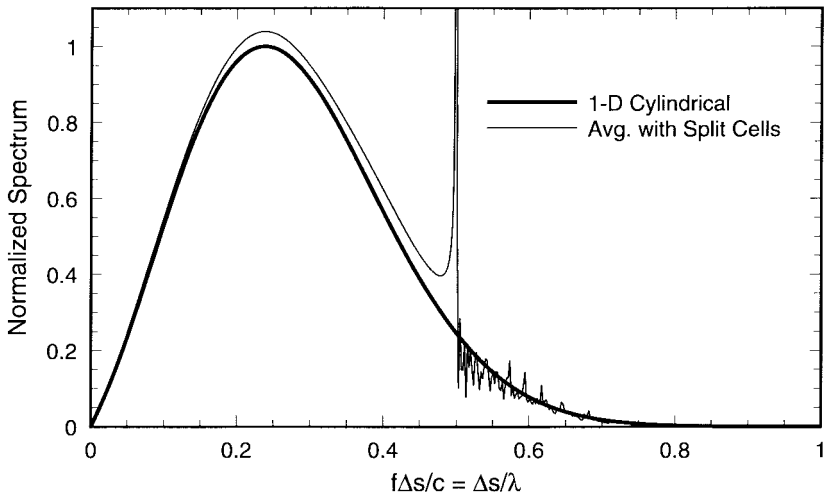

Fig. 6. Normalized spectrum of field at observation point plotted against $f\Delta s/c = \Delta s/\lambda$. Results obtained using an average staircase with cell splitting.

no artifacts associated with artificial boundary conditions are present in the data. Fortunately, although there is some aliasing caused by terminating the simulation while there is some small ringing, this aliasing does not obscure the salient feature of the results: simulations ranging in duration from $t = 60\tau_p$ to $t = 600\tau_p$ all produced a similar spike in the error at $\Delta s = \lambda/2$.

Although the analysis so far has been for a horn with a 12 : 1 slope, similar results are observed for other slopes as well. Fig. 7 shows results obtained using horns with slopes of 8 : 1, 10 : 1, and 14 : 1. Except for the slope, all other parameters are unchanged. The 8 : 1, 10 : 1, and 12 : 1 solutions agree well with their respective analytic solutions (the analytic solutions are shown in Fig. 7 as the thin solid lines) except near or above $\Delta s = \lambda/2$. For the 8 : 1 horn, the amount of energy at $\Delta s = \lambda/2$ is small and, hence, the overall error is likewise small. (The remaining error through the main portion of the spectrum, which is on the order of 2%, is again attributed to the implementation of the feed.) The 14 : 1 solution not only has a pronounced spike at $\Delta s = \lambda/2$, but also underpredicts the values throughout the main portion of the spectrum by approximately 15%.

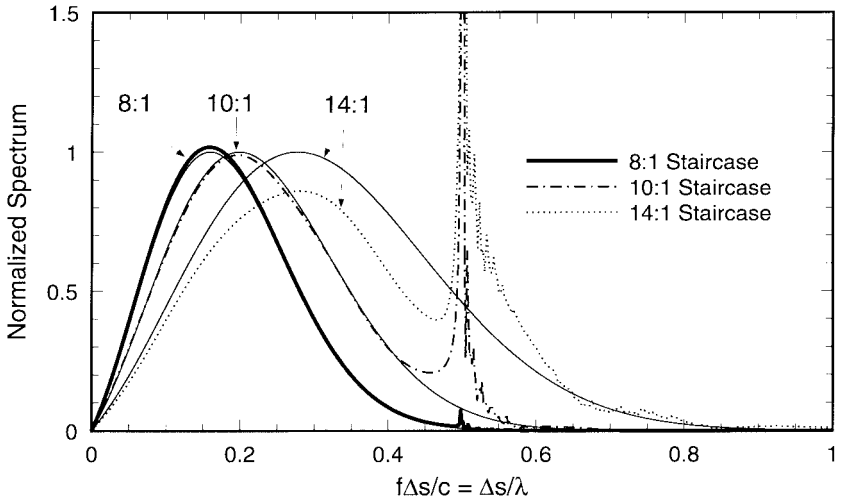

Fig. 7. Normalized spectra versus $\Delta s/\lambda$ for horns with slopes of 8:1, 10:1, and 14:1. Results obtained using an average staircase with cell splitting. The exact solutions for each staircase are given by the thin solid lines.

When using an average staircase with cell splitting, it is difficult to determine precisely *a priori* if the results in the main portion of the pulse will be under or overpredicted. These results depend, in part, on the distance from the observation point to the feed node, the location of the split cells relative to the observation point, and the distance from the feed to the first split cell. All these factors change as the slope changes. Nevertheless, all the results in Figs. 6 and 7 have an erroneous spike at $\Delta s = \lambda/2$ and are poor for $\Delta s > \lambda/2$. The explanation for this is that the grid will establish spurious resonances when the staircase diagonal is a half wavelength. This is a consequence of the phase change over the round-trip distance along the diagonal being 360°. Such resonances can be avoided and high-quality results may be obtained by discretizing a problem such that $\Delta s < \lambda/2$ for all the significant spectral components of the illumination.

It is worth mentioning again that implicit in the analysis given here is the assumption that E_ϕ and E_y are approximately equal along the entire bottom plate of the horn. As the horn slope is increased, this approximation becomes less valid. However, this approximation is well satisfied for all the cases presented here.

IV. Simple Alternative Approaches

As mentioned in the Introduction, many sophisticated schemes have been developed to eliminate staircasing errors. Here, we instead focus on some techniques that can reduce staircasing errors while still being easy to code and computationally inexpensive.

First, we consider perhaps the simplest way to insure that Δs is less than a half wavelength. This is accomplished by merely using cells that do not have a unit aspect ratio. Specifically, for the 12:1 horn, one can (as shown in Fig. 8) use cells with a 12:1 aspect ratio so that the resulting grid has a 1:1 staircase (i.e., the wall of the horn goes over one cell, up one cell, over one cell, and so on). In order to facilitate comparison with the results previously presented

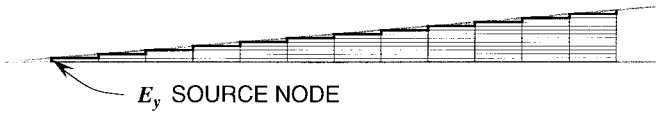

Fig. 8. Outside staircase representation of a 12:1 horn using cells with a 12:1 aspect ratio.

(which had cell areas of 4 mm^2), a grid is constructed with $\Delta x = 4\sqrt{3}$ mm and $\Delta y = 1/\sqrt{3}$ mm so that $\Delta x = 12\Delta y$ and $\Delta x \Delta y = 4$ mm^2.

For these large aspect ratio cells, one can again implement either an outside (as shown in Fig. 8) or an inside staircase approximation of the upper horn wall. Since the staircase is now 1:1, an average staircase cannot be defined. The results for these implementations (run at the Courant limit) are shown in Fig. 9. Again, the outside staircase over predicts the field at the observation point. As before, this is primarily due to ambiguity inherent in the location of the feed node. For the outside staircase, the feed node couples energy into a single cell, which serves to displace the feed closer to the observation point. For the inside staircase, the fields are only slightly under predicted and offset from the analytic solution. The errors are a result of the sensitivity of the model to the feed implementation and the ambiguity caused by the stairstepping adjacent to the feed node. The ambiguity in the vertical direction is much less than in the horizontal direction (since the cells are only one twelfth as high as they are wide), which accounts for the inside staircase providing better results than the outside staircase. Therefore, we conclude that the errors seen here are primarily associated with the feed implementation and should not be associated with general staircasing errors. Significantly, there is no ringing found in the late-time signal for these staircases. For the cells used here, the stairstep length is $\Delta s = \sqrt{48 + 1/3}$ mm. This value of Δs indicates that general staircasing errors will be absent for all spectral components below approximately 20 GHz. Since the driving pulse only has energy up to about 9 GHz, the lack of any late-time ringing in the measured signal is as anticipated.

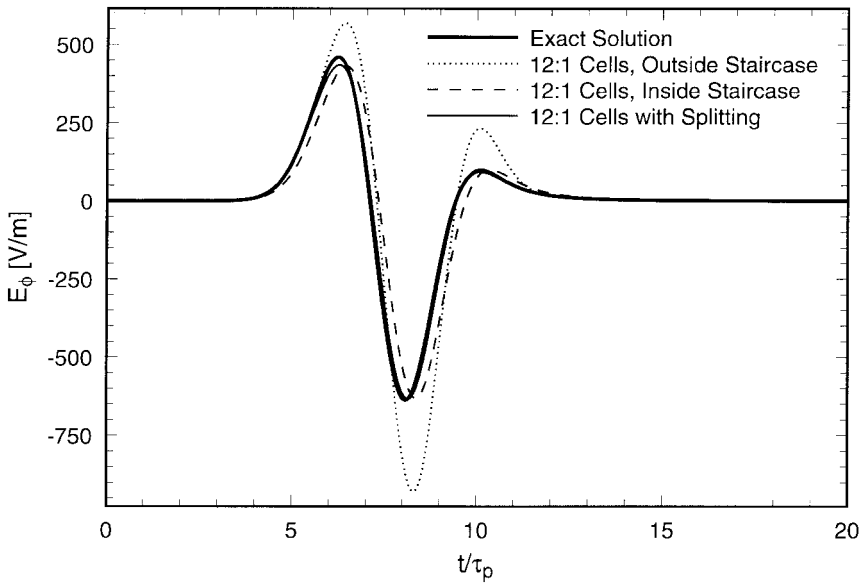

Fig. 9. Electric field 5 cm from the apex using an outside and inside staircase. $\Delta x = 4\sqrt{3}$ mm and $\Delta y = 1/\sqrt{3}$ mm.

By using cells with an aspect ratio that mimics the slope of the upper horn wall, that wall is realized with a $1:1$ staircase. By splitting each cell along the wall boundary, the scheme described by Mezzanotte *et al.* [9] is obtained (see [16] and [17] and the references therein for alternative descriptions of this approach). The results obtained using this scheme are also plotted in Fig. 9 and are indistinguishable from the analytic solution except for a slight discrepancy near $t = 6\tau_p$. This cell-splitting scheme splits every cell along the metal boundary and, therefore, cannot generally be used when the spatial step sizes are the same in all directions throughout the grid. In the previous section where the spatial step sizes were the same, only every twelfth cell could be split. Thus, the scheme of Mezzanotte *et al.* requires a global distortion of the cell sizes in order to ensure that boundaries can be modeled with a $1:1$ staircase. Since the temporal step size is essentially dictated by the smallest spatial step, the small vertical step size needed here results in run times that are much longer than those used in the previous section. Furthermore, in general problems the inherent numerical grid dispersion and anisotropy (which were purposely avoided in this study) caused by these large aspect ratio cells may be significant.

Finally, the contour path (CP) FDTD scheme, the modified CPFDTD scheme, and the scheme proposed by Dey are considered. The CPFDTD approach typically uses the traditional uniform Cartesian grid FDTD technique everywhere except at material boundaries where conformal cells are used [4], [10]. The scheme is simple to implement in two dimensions and has been implemented in three. Furthermore, the CPFDTD scheme is relatively low cost since the number of modified cells is typically much less than the total number of cells and the operation count associated with modified cells is low. However, as originally published, the stability of the CPFDTD scheme is not guaranteed owing to the use of nonreciprocal "borrowing" of field values (i.e., the nearest-neighbor approximation). To ensure stability, Railton *et al.* [13] and Railton and Craddock [18], [19] have put forward a modified CPFDTD scheme that uses a reciprocal borrowing of fields. For the horns studied here, no instability was observed using the original CPFDTD scheme. Thus, the question arose if the modified CPFDTD (in addition to ensuring stability) also provided accuracy above that obtained using the original scheme. The Dey method does not involve any borrowing and is arguably the simplest conformal technique to implement. All electric field update equations are the same as those used in the conventional FDTD scheme, while the magnetic field update equations for cells adjacent to a metallic boundary are only slightly modified to include geometric factors. The "cost" of this simple scheme is a reduced Courant number.

Fig. 10 shows the results obtained using the two contour path (CP) techniques, the Dey method, and the analytic solution. The spatial and temporal step sizes used for the CP approaches are the same as those used in the previous section (i.e., $\Delta x = \Delta y = 2$ mm and Δt at the Courant limit). The same step size was used in the Dey method, but the Courant number was reduced to half the limit in order to obtain a stable result. When viewing the entire pulse, the four curves are indistinguishable. In the inset box, a portion of the tail is expanded vertically by a factor of approximately 1000. At this scale, the original contour path scheme is seen to deviate slightly more from the analytic result than do the others. Thus, the modified CP scheme does appear to provide some additional accuracy over the original scheme. The Dey scheme, despite its simplicity, provides results that are comparable to that of the modified CP scheme (and superior to those of the original CP scheme). As expected, the Fourier transform of these results, as well as those of the large aspect ratio cells, do not have any significant error at $\Delta s = \lambda/2$.

V. Conclusions

By carefully implementing the feed of a horn and comparing with the analytic solution, meaningful conclusions can

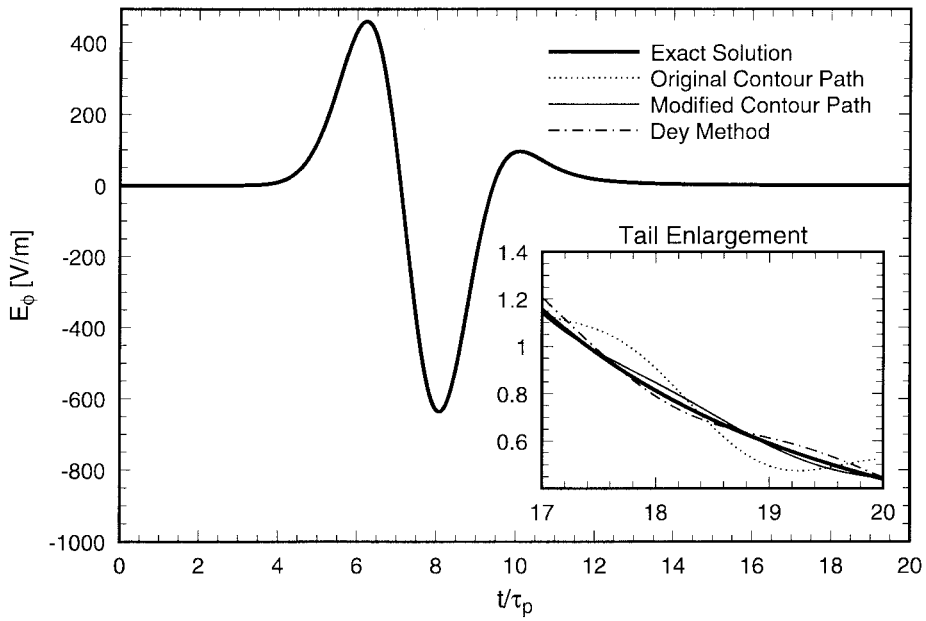

Fig. 10. Electric field 5 cm from the apex using the original and modified contour path schemes and the conformal Dey method. $\Delta x = \Delta y = 2$ mm.

be drawn about the level of discretization that is needed to obtain accurate results. To avoid general staircasing errors, the grid must be constructed so that $\Delta s < \lambda/2$ for all significant frequencies in the excitation, where Δs is the stairstep diagonal length. Of course, this level of discretization does not, in itself, guarantee an accurate solution. Problems in which small or subcellular structures are important will require special consideration. This was made clear by the errors observed using the outside and inside staircases with the large aspect ratio cells. In that case, although general staircasing errors associated with the upper horn plate were absent, there were errors caused by the step discontinuities in the immediate vicinity of the feed node. Thus, one can consider the rule-of-thumb given here as a necessary rather than a sufficient condition for an accurate solution.

It was shown that some simple schemes can be used to reduce or eliminate staircasing errors. By using large aspect ratio cells and modeling the boundaries with a 1:1 staircase, most staircasing errors can be eliminated. However, to eliminate the errors associated with staircasing in the immediate vicinity of the feed node, it was further necessary to split the boundary cells. Another scheme—the original contour path FDTD approach—significantly reduced staircasing errors. The modified contour path approach, which was put forward as a solution to instabilities in the original scheme, provided some additional accuracy. The conformal method recently presented by Dey and Mittra, which is perhaps the simplest conformal technique to implement, was found to yield results comparable to the modified contour path method.

Although the analysis conducted here was performed in two dimensions, the conclusions have been found to be consistent with the analysis of 3-D horn antennas where flat plates were slanted with respect to the principle grid planes.

ACKNOWLEDGMENT

The authors would like to thank Dr. G. S. Smith, Georgia Institute of Technology, Atlanta, for providing the analytic solution.

REFERENCES

[1] K. S. Yee, "Numerical solution of initial boundary value problems involving Maxwell's equations in isotropic media," *IEEE Trans. Antennas Propagat.*, vol. AP-14, no. 3, pp. 302–307, May 1966.
[2] R. Holland, "Finite difference solutions of Maxwell's equations in generalized nonorthogonal coordinates," *IEEE Trans. Nucl. Sci.*, vol. NS-30, no. 6, pp. 4589–4591, Dec. 1983.
[3] M. A. Fusco, M. V. Smith, and L. W. Gordon, "A three-dimensional FDTD algorithm in curvilinear coordinates," *IEEE Trans. Antennas Propagat.*, vol. 39, pp. 1463–1471, Oct. 1991.
[4] T. G. Jurgens, A. Taflove, K. Umashankar, and T. G. Moore, "Finite-difference time-domain modeling of curved surfaces," *IEEE Trans. Antennas Propagat.*, vol. 40, no. 4, pp. 357–366, Apr. 1992.
[5] J.-F. Lee, R. Palandech, and R. Mittra, "Modeling three-dimensional discontinuities in waveguides using nonorthogonal FDTD algorithm," *IEEE Trans. Microwave Theory Tech.*, vol. 40, no. 2, pp. 346–352, Feb. 1992.
[6] N. K. Madsen, "Divergence preserving discrete surface integral methods for Maxwell's curl equations using nonorthogonal unstructured grids," *J. Comput. Phys.*, vol. 119, pp. 34–45, 1995.
[7] A. C. Cangellaris and D. B. Wright, "Analysis of the numerical error caused by the stair-stepped approximation of a conducting boundary in FDTD simulations of electromagnetic phenomena," *IEEE Trans. Antennas Propagat.*, vol. 39, pp. 1518–1525, Oct. 1991.
[8] R. Holland, "Pitfalls of staircase meshing," *IEEE Trans. Electromagn. Compat.*, vol. 35, no. 4, pp. 434–439, Nov. 1993.
[9] P. Mezzanotte, L. Roselli, and R. Sorrentino, "A simple way to model curved metal boundaries in FDTD algorithm avoiding staircase approximation," *IEEE Microwave Guided Wave Lett.*, vol. 5, no. 8, pp. 267–269, Aug. 1995.
[10] T. G. Jurgens and A. Taflove, "Three-dimensional contour FDTD modeling of scattering from single and multiple bodies," *IEEE Trans. Antennas Propagat.*, vol. 41, pp. 1703–1708, Dec. 1993.
[11] S. Dey and R. Mittra, "A locally conformal finite difference time domain (FDTD) algorithm for modeling 3-D objects with curved surfaces," in *IEEE Antennas Propagat. Soc. Int. Symp.*, Montréal, Canada, July 1997, vol. 4, pp. 2172–2175.
[12] S. Dey, R. Mittra, and S. Chebolu, "A technique for implementing the FDTD algorithm on a nonorthogonal grid," *Microwave Opt. Technol. Lett.*, vol. 14, no. 4, pp. 213–215, 1997.

[13] C. J. Railton, I. J. Craddock, and J. B. Schneider, "The analysis of general two-dimensional PEC structures using a modified CPFDTD algorithm," *IEEE Trans. Microwave Theory Tech.*, vol. 44, pp. 1728–1733, Oct. 1996.
[14] K. L. Shlager, G. S. Smith, and J. G. Maloney, "Accurate analysis of TEM horn antennas for pulse radiation," *IEEE Trans. Electromagn. Compat.*, vol. 38, no. 3, pp. 414–423, Aug. 1996.
[15] A. Taflove, *Computational Electrodynamics: The Finite-Difference Time-Domain Method*. Boston, MA: Artech House, 1995.
[16] T. Weiland, "Comment on 'A simple way to model curved metal boundaries in FDTD algorithm avoiding staircase approximation,'" *IEEE Microwave Guided Wave Lett.*, vol. 6, no. 4, pp. 183–184, Apr. 1996.
[17] P. Mezzanotte and L. Roselli, "Reply to comment on 'A simple way to model curved metal boundaries in FDTD algorithm avoiding staircase approximation,'" *IEEE Microwave Guided Wave Lett.*, vol. 6, no. 4, p. 184, Apr. 1996.
[18] C. J. Railton and I. J. Craddock, "Analysis of general 3-D PEC structures using improved CPFDTD algorithm," *Electron. Lett.*, vol. 31, no. 20, pp. 1553–1554, 1995.
[19] ——, "Stabilized CPFDTD algorithm for the analysis of arbitrary 3-D PEC structures," *Proc. Inst. Elect. Eng. Microwave Antennas Propagat.*, vol. 143, pt. H, no. 5, pp. 367–372, Oct. 1996.

John B. Schneider received the B.S. degree in electrical engineering (*summa cum laude*) from Tulane University, New Orleans, LA, in 1983, and the M.S. and Ph.D. degrees in electrical engineering from the University of Washington, Seattle, in 1985 and 1991, respectively.

He is currently an Assistant Professor in the School of Electrical Engineering and Computer Science, Washington State University. His research interests include the use of computational methods to analyze acoustic, elastic, and electromagnetic wave propagation.

Dr. Schneider received the Office of Naval Research Young Investigator Award in 1996.

Kurt L. Shlager (M'81) received the B.S.E.E. degree from Southeastern Massachusetts University, North Dartmouth, MA, the M.S.E.E. degree from Tufts University, Medford, MA, and the Ph.D. degree from the Georgia Institute of Technology, Atlanta, GA, in 1985, 1987, and 1995, respectively.

From 1985 to 1986, he was with the Antenna Development Group at GTE Government Systems, Westborough, MA. He was with Lockheed Missiles and Space Company, Sunnyvale, CA, from 1987 to 1990, doing research and development in electromagnetic scattering. In 1995 he joined the Antenna Systems Laboratory of TRW Space and Electronics Group, Redondo Beach, CA. He returned to Lockheed-Martin Missiles and Space Company in 1996, where he is currently involved in antenna analysis and design. His research interests are in computational electromagnetics, including the finite-difference time-domain method, electromagnetic scattering, and antenna analysis and design.

Dr. Shlager is a member of the Eta Kappa Nu Honor Society.